INTERNATIONAL JOURNAL FOR NUMERICAL METHODS IN FLUIDS
Int. J. Numer. Meth. Fluids 2008; **57**:861–876
Published online 6 November 2007 in Wiley InterScience (www.interscience.wiley.com). DOI: 10.1002/fld.1655

Transient free convection with mass transfer MHD micropolar fluid in a porous plate by the network method

Joaquín Zueco*, †

Department of Thermal Engineering and Fluids, Technical University of Cartagena, Campus Muralla del Mar, Cartagena 30202, Spain

SUMMARY

The transient problem of coupled heat and mass transfer of a micropolar fluid in magneto-hydrodynamic free convection from a vertical infinite porous plate with an exponentially decaying heat generating considering the viscous dissipation and ohmic heating effects is studied. Joule heating must be considered when the viscous dissipation and the Prandtl number are large. The non-dimensional equations for the conservation of mass, momentum, energy and concentration are solved by means a numerical technique based on electric analogy (network simulation method). This method provides the numerical response of the system by running the network in circuit resolution software with the solution to both transient and steady-state problems at the same time, and its programming does not require manipulation of the sophisticated mathematical software that is inherent in other numerical methods. The effects of the material parameters, viscous dissipation, internal generation and Joule heating on velocity, angular momentum and temperature fields across the boundary layer are investigated. In addition, the skin-friction coefficient, couple stress coefficient, Nusselt number and Sherwood number are shown in tabular form. The numerical results for velocity and temperature distributions of micropolar fluids are compared with the corresponding flow problems for a Newtonian fluid. Copyright © 2007 John Wiley & Sons, Ltd.

Received 13 July 2007; Revised 20 September 2007; Accepted 2 October 2007

KEY WORDS: free convection; micropolar fluid; mass transfer; viscous dissipation; network model; internal generation

INTRODUCTION

In many practical applications, for example, magneto-hydrodynamic (MHD) generators, extrusion of polymer fluids, plasma studies, nuclear reactors, oil exploration and geothermal energy extraction, it is very important to study the flow and heat transfer for an electrically conducting polar fluid past a porous plate under the influence of a transverse magnetic field. Another application is

*Correspondence to: Joaquín Zueco, Department of Thermal Engineering and Fluids, Technical University of Cartagena, Campus Muralla del Mar, Cartagena 30202, Spain.
†E-mail: joaquin.zueco@upct.es

in industrial manufacturing processes, where it may be necessary to consider internal heat generation to consolidate production, as well applications in fire and combustion modelling. In these processes, the heat transfer rates can be controlled by means of a magnetic field, and knowledge of the unsteady and stationary heat transfer is important. The combination of the effects of internal heat generation, Joule heating and viscous dissipation in the MHD process with micropolar fluids is studied here. It was shown by Gebhart [1] that the viscous dissipation effect plays an important role in free convection in various devices that are subjected to large deceleration, or which operate at high rotative speeds and also in strong gravitational field processes on large scales and geological process. The heat due to viscous dissipation in the energy equation is very small and is neglected. However, when the gravitational force is intensive or when the Prandtl number of the fluid is very high, the viscous dissipative effects cannot be neglected. These effects mean that this problem is governed by a coupled non-linear system of partial differential equations; hence, that exact solutions are not possible. It is therefore necessary to solve the problem by numerical means using, for example, the network simulation method (NSM) as in this study.

Eringen [2] developed the theory that the local effects arising from the microstructure and the intrinsic motion of the fluid elements should be taken into account. The theory is expected to provide a mathematical model for the non-newtonian fluid behaviour observed in certain man-made liquids, such as polymers, lubricants, fluids with additives, paints, animal blood, colloidal and suspension solutions, etc. The presence of dust or smoke, particularly in a gas, may also be modelled using micropolar fluid dynamics. Later, Eringen [3] extended the theory of thermo-micropolar fluids and derived the constitutive laws for fluids with microstructures.

Ibraim and Hassanien [4] solved the mixed convection boundary-layer flow of a micropolar fluid on a horizontal flat plate with power law variation in surface temperature. El-Hakiem [5] obtained a similarity solution for the flow of a micropolar fluid along an isothermal vertical plate with an exponentially decaying heat generation term and thermal dispersion. Chang [6] investigated the wall plume associated with natural convection flow in micropolar fluids. Gorla *et al.* [7] developed a numerical scheme to solve the steady free convection from a vertical isothermal plate in a strong cross magnetic field immersed in a micropolar fluid. El-Hakiem *et al.* [8] presented an analysis for the effect of viscous and Joule heating on MHD-free convection flow over a non-isothermal surface in a micropolar fluid.

El-Amin [9, 10] obtained numerical solutions for the problem of steady free convection and mass transfer flow in a micropolar fluid with constant suction, studying the combined effect of internal heat generation and magnetic field. Ibrahim *et al.* [11] solved the unsteady MHD micropolar fluid flow and heat transfer over a vertical porous plate through a porous medium in the presence of thermal and mass diffusion with a constant heat source. Mansour *et al.* [12] studied the combined heat and mass transfer in MHD of a micropolar fluid boundary-layer flow past a circular cylinder surface with non-uniform heat and mass flux. Eldabe and Mahmoud [13] solved the problem that involves the heat and mass transfer in a hydromagnetic flow of a micropolar fluid past a stretching surface with Ohmic heating and viscous dissipation. Abo-Eldahad and El Aziz [14] studied the effects of viscous dissipation and Joule heating on MHD-free convection flow past a semi-infinite vertical flat plate in the presence of the combined effect of Hall and ion-slip currents for the case of power law variation of the wall temperature.

The aim of the present work is to solve the unsteady natural convection along an infinite vertical porous plate with a constant suction velocity and subject to a transverse constant external magnetic field, taking into account the internal heat generation, Joule heating, the viscous dissipation and the mass transfer of a viscous electrically conducting micropolar fluid, by means of a new numerical

DOI: 10.1002/fld

technique based on electrical analogy, NSM. Firstly, a spatial discretization is applied to the transient boundary-layer equations, and a set of ordinary differential equations are obtained, one for each control volume. Electrical–thermal–motion analogy provides a network model that is solved by means of a very common program used to simulate electrical circuits, PSPICE [15]. The main advantage of the method is that time derivatives are not replaced by finite differences (similar to the method of lines [16, 17]), but only require finite-difference schemes for the spatial variable.

NSM has been successfully applied to solving several heat transfer problems; for example, Zueco [18, 19] studied the effect of the viscous dissipation on a vertical channel and on a semi-infinite vertical flat plate submitted to a constant heat flux in the presence of a magnetic field, respectively. Zueco and Campo [20] solved transient radiative transfer between the thick walls of an enclosure by means of a new network model that can be applied to different radiation problems. Zueco and Alhama [21] developed an iterative algorithm for estimating the dependence of temperature of the specific heat and thermal conductivity of fluids.

MATHEMATICAL MODEL

We consider a two-dimensional unsteady natural convection with mass transfer flow of a micropolar and incompressible fluid past an infinite vertical porous plate submitted to a transverse magnetic field. The fluid has an internal volumetric heat generation. The x-axis is vertically upwards and the y-axis is the coordinate perpendicular to x. Outside the plate, the quiescent ambient fluid is at a lower constant temperature T_∞, with $(u, v, 0)$ being the velocity field and $(0, 0, n)$ microrotation, u and v denote, respectively, the velocity components in the x and y directions and n the microrotation in the direction normal to both x and y. A uniform magnetic field is assumed to exist in the direction normal to the surface. All fluid properties are considered to be constant, except the density variation with temperature, which is considered only in the body force term. It is considered that the viscous dissipation and the interaction of the induced axial magnetic field with the flow are negligible compared with the interaction of the applied magnetic field B with the flow. Besides, it is assumed that there is no chemical reaction between the diffusing species and the fluid. The transient two-dimensional flow can be shown to be governed by the following boundary-layer equations (including viscous dissipation and Joule heating):

Continuity equation:

$$\partial v/\partial y = 0 \tag{1}$$

Momentum equation:

$$\partial u/\partial t + v\partial u/\partial y = (v + K/\rho)\partial^2 u/\partial y^2 + \beta g(T - T_\infty) + \beta^* g(c - c_\infty) + K/\rho \partial n/\partial y - u\sigma B_0^2/\rho \tag{2}$$

Energy of angular moment:

$$\rho j \partial n/\partial t + v\rho j \partial n/\partial y = \gamma \partial^2 n/\partial y^2 - K(2n + \partial u/\partial y) \tag{3}$$

Energy equation:

$$\partial T/\partial t + v\partial T/\partial y = \alpha \partial^2 T/\partial y^2 + (\mu + K)/\rho c_p (\partial u/\partial y)^2 + Q + u^2 \sigma B_0^2 \tag{4}$$

DOI: 10.1002/fld

Mass equation:

$$\partial c/\partial t + v\partial c/\partial y = D\partial^2 c/\partial y^2 \tag{5}$$

where υ is the kinematic viscosity, ρ the density, K the vortex viscosity, g the acceleration due to gravity, β the coefficient of volume expansion, β^* the coefficient of volume expansion with concentration, j the microinertia per unit mass, γ the spin gradient viscosity, T the temperature in the boundary layer, α the thermal diffusivity, μ the dynamic viscosity, c_p the specific heat, Q the volumetric heat generation, σ the electrical conductivity of the fluid, B_0 the magnetic induction, c and c_∞ the concentrations in the boundary layer and free stream, respectively, and D the chemical molecular diffusivity. The initial and boundary conditions are

$$t \leqslant 0; \quad u=0, \ n=0, \ T=T_\infty, \ c=c_\infty \tag{6a}$$

$$t>0; \quad u=0, \ n=-m\partial u/\partial y, \ T=T_w, \ c=c_w \quad \text{at } y=0 \tag{6b}$$

$$t>0; \quad u\to 0, \ n\to 0, \ T\to T_\infty, \ c\to c_\infty \quad \text{as } y\to\infty \tag{6c}$$

where T_w and c_w are the temperature and concentration on the limiting surface. $m=0$ represents the case of concentration particle flows in which the microelements close to the wall are not able to rotate, whereas for $m=\frac{1}{2}$ and 1, the microrotation term is greater and induces flow enhancement. The integration of Equation (1) gives

$$v=-v_0 \tag{7}$$

where v_0 (>0) is the constant suction of the fluid through the porous limiting surface.

The above equations are expressed in a non-dimensional form by employing the following boundary-layer dimensionless variables:

$$\begin{gathered} Y=v_0 y/\upsilon, \quad U=u/v_0, \quad \tau=tv_0^2/\upsilon, \quad \theta=(T-T_\infty)/(T_w-T_\infty), \quad C=(c-c_\infty)/(c_w-c_\infty) \\ N=\upsilon n/v_0^2, \quad Pr=\upsilon/\alpha, \quad Ec=v_0^2/c_p(T_w-T_\infty), \quad Gr^*=\upsilon g\beta(T_w-T_\infty)/v_0^3 \\ Gm=\upsilon g\beta^*(c_w-c_\infty)/v_0^3, \quad M=\sigma B_0^2\upsilon/\rho v_0^2, \quad \Lambda=K/\mu, \quad \lambda=\gamma/\mu j, \quad B=\upsilon^2/jv_0^2 \end{gathered} \tag{8}$$

where Gr^* is the modified Grashof number, Gm is the buoyancy ratio parameter, Sc is the Schmidt number, M is the magnetic parameter, Ec is the Eckert number and Λ is the couple parameter.

The volumetric heat generation is

$$Q=\Psi(y)(T_w-T_\infty)v_0^2/\upsilon \tag{9}$$

where $\Psi(y)$ is a function of the y-coordinate or simply a constant. We can choose any expression for $\Psi(y)$, regardless of whether a similarity solution exists. In this work, we choose $\Psi(y)=A\mathrm{e}^Y$ to compare the results with those of El-Amin [9], with A being a constant value denominated heat generation parameter.

Then, the governing equations reduce to the following non-dimensional boundary-layer equations:

$$\partial U/\partial\tau - \partial U/\partial Y = (1+\Lambda)\partial^2 U/\partial Y^2 + Gr\,\theta + Gm\,C + \Lambda\partial N/\partial Y - MU \tag{10a}$$

$$\partial N/\partial\tau - \partial N/\partial Y = \lambda\partial^2 N/\partial Y^2 - \Lambda B(\partial U/\partial Y + 2N) \tag{10b}$$

DOI: 10.1002/fld

$$Pr\,\partial\theta/\partial\tau - Pr\,\partial\theta/\partial Y = \partial^2\theta/\partial Y^2 + Ec\,Pr(1+\Lambda)(\partial U/\partial Y)^2 + Pr\,A + Pr\,Ec\,MU^2 \tag{10c}$$

$$\partial C/\partial\tau - \partial C/\partial Y = Sc^{-1}\partial^2 C/\partial Y^2 \tag{10d}$$

The dimensionless initial and boundary conditions become

$$\tau \leqslant 0; \quad U = N = \theta = C = 0 \tag{11a}$$

$$\tau > 0; \quad U = 0, \ \ N = -m\partial U/\partial Y, \ \ \theta = 1, \ \ C = 1 \quad \text{at } Y = 0 \ \ \forall X \tag{11b}$$

$$\tau > 0; \quad U \to 0, \ \ N \to 0, \ \ \theta \to 0, \ \ C \to 0 \quad \text{as } Y \to \infty \ \ \forall X \tag{11c}$$

NUMERICAL SCHEME

NSM is used to solve the problem. The discretization of the boundary-layer equations is based on the finite-difference formulation and electrical analogy, where only a discretization of the spatial coordinates is necessary, while time remains a real continuous variable, similar to the method of lines. Hence, the imminent advantage of this method of no mathematical manipulations in the discretization of the time coordinate, which are necessary for most of the numerical methods used currently, since the code does this work. The difference with the method of lines is that the technique used for solving the finite-difference equations discretize spatially (with time as a continuous variable); the method of lines uses a direct mathematical software, while the NSM uses a simulator of electric circuits, PSPICE. Method of lines benefits from the recent advances in the resolution of equation differential ordinary by computer, while NSM makes use of the advances in the computerized resolution of electric circuits.

To ensure an accurate transient analysis, the time step must be controlled to produce an acceptable amount of local truncation error at each time point. The implementation of a local truncation error time-step control with trapezoidal integration (with an order two accurate) is applied in the transient analysis. The algorithms that are employed in PSPICE are presented in detail, and the performance of these methods is compared with the performance of other available techniques in the thesis of Nagel [22]. NSM simulates the behaviour of unsteady electric circuits by means of resistors, capacitors and non-linear devices that seek to resemble thermal systems governed by unsteady linear or non-linear equations. This method has been applied successfully to a great variety of linear and non-linear transport problems [18–21].

The electrical analogy relates the electrical current (J) with the velocity flux ($\partial U/\partial Y$), micro-rotation flux ($\partial N/\partial Y$), temperature flux ($\partial\theta/\partial Y$) and the concentration flux ($\partial C/\partial Y$), while the electrical potential (Φ) is equivalent to U, N, θ and C for the momentum, angular moment, energy and mass equation, respectively. For each non-dimensional boundary-layer equation, an electrical network circuit is developed (Figure 1), where a previous spatial discretization is realized. The whole network must be converted into an adequate program that is solved by a computer code (electric circuits simulator), PSPICE [15]. For the transient analysis, PSPICE uses the numerical implicit integration formulae (trapezoidal integration) with an order two accurate, besides a central difference being used for the approximation of first and second spatial derivatives; therefore, a second order of accuracy of the spatial discretization is obtained. Time remains as a continuous variable, which results in greater accuracy and no time interval needs to be established by the programmer; PSPICE imposed and adjusted continuously automatically this parameter to reach a

DOI: 10.1002/fld

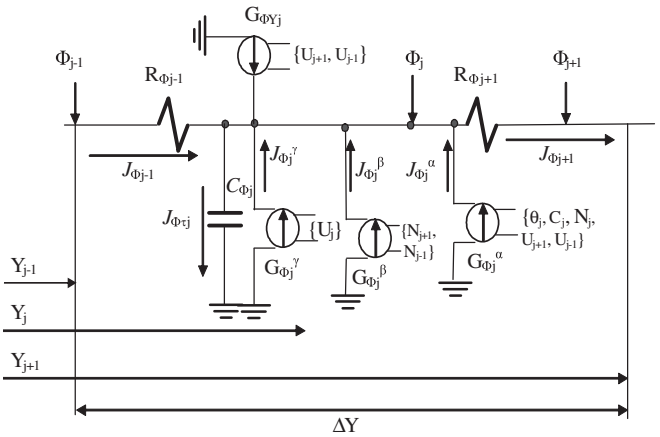

Figure 1. Network model of the control volume.

convergent solution in each iteration, according to the given stability and convergence requirements (internal to the code PSPICE). The convergence criterion used by PSPICE requires that the vector of circuit variables V_{t+1} agrees with the prior solution V_t within a specified tolerance; hence, it is necessary that each component of the unknown vector $V_t(n)$ satisfies the following equation:

$$|\Phi_{t+1}(n)-\Phi_t(n)|<\varepsilon_a+\varepsilon_r \mathrm{Min}\{|\Phi_t(n)|, |\Phi_{t+1}(n)|\} \tag{12}$$

where ε_a is an absolute tolerance and ε_r is a relative tolerance. Values of 10^{-4} for ε_a and of $50\,\mu V$ for ε_r produce acceptable results in most cases. If a time-step solution does not converge, the time step usually can be reduced until the solutions converge. This time-step reduction is necessary to maintain a reasonable level of truncation error in the analysis. Details of the local truncation errors can been found in the thesis of Nagel [22].

Another remarkable advantage of the NSM is that it provides both voltage and electric current; hence, the temperatures, velocities, concentrations and heat fluxes, velocities fluxes and concentration fluxes are obtained immediately, with no subsequent numerical manipulation. Besides, generally few programming rules are necessary since the number of electrical devices that make up the network is very small, and a wide library of electrical components is available for the future simulation of more complex processes.

Design of the network model

In the network theory, the viability of a network model implies

(i) The existence of a network independent of time.
(ii) The existence of a magnitude $J_{j,j-1}$-denominated flux associated with each branch that connects the nodes j and $(j-1)$. This flux follows the Kirchhoff law for currents.
(iii) The existence of a magnitude $\Phi_{j,j-1}$-denominated potential, associated with each node, so that the difference $\Phi_{j,j-1}=\Phi_j-\Phi_{j-1}$, is according to the Kirchhoff law of voltages.

It is necessary to develop four network models, one for every equation (momentum balance, angular moment balance, energy balance and mass balance). The design of the network models

DOI: 10.1002/fld

(Figure 1) is as follows, where the values of the devices that build each network model are shown in Table I. The finite-difference differential equations are obtained in this section. A second-order central difference scheme has been used to discretize the boundary-layer equations, $2\Delta Y$ being the thickness of the elemental cell:

$$(\partial\Phi/\partial Y)_j \approx (\Phi_{j+1}-\Phi_{j-1})/(2\Delta Y) \tag{13}$$

$$(\partial^2\Phi/\partial Y^2)_j \approx (\Phi_{j+1}+\Phi_{j-1}-2\Phi_j)/\Delta Y^2 = 1/\Delta Y[(\Phi_{j-1}-\Phi_j)/\Delta Y-(\Phi_j-\Phi_{j+1})/\Delta Y] \tag{14}$$

Introducing expressions (13)–(14) in the non-dimensional equations (10a)–(10d), the finite-difference differential equations are

(i) *Momentum equation*:

$$\begin{aligned}\Delta Y/(1+\Lambda)\,\mathrm{d}U_j/\mathrm{d}\tau-(U_{j+1}-U_{j-1})/2(1+\Lambda)\\ =(U_{j-1}-U_j)/\Delta Y-(U_j-U_{j+1})/\Delta Y+\Delta Y/(1+\Lambda)(Gr\,\theta_j+Gm\,C_j)\\ +\Lambda(N_{j+1}-N_{j-1})/2(1+\Lambda)-\Delta Y/(1+\Lambda)MU_j\end{aligned} \tag{15}$$

Defining the currents,

$$J_{U\tau j}=\Delta Y/(1+\Lambda)\,\mathrm{d}U_j/\mathrm{d}\tau \tag{16a}$$

$$J_{UYj}=(U_{j+1}-U_{j-1})/2(1+\Lambda) \tag{16b}$$

$$J_{Uj-1}=(U_{j-1}-U_j)/\Delta Y \tag{16c}$$

$$J_{Uj+\Delta Y}=(U_j-U_{j+1})/\Delta Y \tag{16d}$$

$$J^{\alpha}_{Uj}=\Delta Y/(1+\Lambda)(Gr\,\theta_j+Gm\,C_j) \tag{16e}$$

$$J^{\beta}_{Uj}=\Lambda(N_{j+1}-N_{j-1})/2(1+\Lambda) \tag{16f}$$

$$J^{\gamma}_{Uj}=\Delta Y/(1+\Lambda)MU_j \tag{16g}$$

Equation (15) can be expressed in the form of Kirchhoff's law:

$$J_{U\tau j}-J_{UYj}-J_{Uj-1}+J_{Uj+1}-J^{\alpha}_{Uj}-J^{\beta}_{Uj}+J^{\gamma}_{Uj}=0 \tag{17}$$

(ii) *Equation of angular moment*:

$$\begin{aligned}\Delta Y/\lambda\,\mathrm{d}N_j/\mathrm{d}\tau-(N_{j+1}-N_{j-1})/2\lambda=(N_{j-1}-N_j)/\Delta Y-(N_j-N_{j+1})/\Delta Y\\ -\Lambda B[(U_{j+1}-U_{j-1})+2\Delta Y N_j]/\lambda\end{aligned} \tag{18}$$

Defining the currents,

$$J_{N\tau j}=\Delta Y/\lambda\,\mathrm{d}N_j/\mathrm{d}\tau \tag{19a}$$

$$J_{Nyj}=(N_{j+1}-N_{j-1})/2\lambda \tag{19b}$$

DOI: 10.1002/fld

Table I. Expressions of the devices of the network model (electrical analogy).

	Φ	$C_{\Phi j}$	$R_{\Phi j\pm\Delta Y}$	$G_{\Phi Y j}$	$G^{\alpha}_{\Phi j}$	$G^{\beta}_{\Phi j}$	$G^{\gamma}_{\Phi j}$
Momentum	U	$\Delta Y/(1+\Lambda)$	ΔY	$(U_{j+1}-U_{j-1})/2(1+\Lambda)$	$\Delta Y\ (Gr\theta_j+GmC_j)/(1+\Lambda)$	$\Lambda(N_{j+1}-N_{j-1})/2(1+\Lambda)$	$-\Delta Y MU_j/(1+\Lambda)$
Angular	N	$\Delta Y/\lambda$	ΔY	$(N_{j+1}-N_{j-1})/2\lambda$	$-\Lambda B[(U_{j+1}-U_{j-1})/2+2\Delta Y N_j]/\lambda$	—	—
Energy	θ	$\Delta Y Pr$	ΔY	$(\theta_{j+1}-\theta_{j-1})Pr/2$	$(U_{j+1}-U_{j-1})^2 EcPr\ (1+\Lambda)/4\Delta Y$	$\Delta Y PrA$	$\Delta Y PrEcMU_j^2$
Mass	C	$\Delta Y Sc$	ΔY	$(C_{j+1}-C_{j-1})Sc/2$	—	—	—

DOI: 10.1002/fld

$$J_{Nj+1}=(N_j-N_{j+1})/\Delta Y \tag{19c}$$

$$J_{Nj-1}=(N_{j-1}-N_j)/\Delta Y \tag{19d}$$

$$J^{\alpha}_{N\Delta j}=\Lambda B[(U_{j+1}-U_{j-1})/2+2\Delta Y N_j]/\lambda \tag{19e}$$

Equation (18) can be expressed in the form of Kirchhoff's law:

$$J_{N\tau j}-J_{NYj}-J_{Nj-1}+J_{Nj+1}+J^{\alpha}_{Nj}=0 \tag{20}$$

(iii) *Energy equation*:

$$\begin{aligned}&\Delta Y\,Pr\,\mathrm{d}\theta_j/\mathrm{d}\tau-Pr(\theta_{j+1}-\theta_{j-1})/2\\&=(\theta_{j-1}-\theta_j)/\Delta Y-(\theta_j-\theta_{j+1})/\Delta Y\\&\quad+Ec\,Pr(1+\Lambda)(U_{j+1}-U_{j-1})^2/4\Delta Y+\Delta Y\,Pr\,A+\Delta Y\,Pr\,Ec\,MU_j^2\end{aligned} \tag{21}$$

Defining the currents,

$$J_{\theta\tau j}=\Delta Y\,Pr\,\mathrm{d}\theta_j/\mathrm{d}\tau \tag{22a}$$

$$J_{\theta Yj}=Pr(\theta_{j+1}-\theta_{j-1})/2 \tag{22b}$$

$$J_{\theta j-1}=(\theta_{j-\Delta Y}-\theta_j)/\Delta Y \tag{22c}$$

$$J_{\theta j+1}=(\theta_j-\theta_{j+1})/\Delta Y \tag{22d}$$

$$J^{\alpha}_{\theta j}=Ec\,Pr(1+\Lambda)(U_{j+1}-U_{j-1})^2/4\Delta Y \tag{22e}$$

$$J^{\beta}_{\theta j}=\Delta Y\,Pr\,A \tag{22f}$$

$$J^{\gamma}_{\theta j}=\Delta Y\,Pr\,Ec\,MU_j^2 \tag{22g}$$

Equation (21) can be expressed in the form of Kirchhoff's law:

$$J_{\theta\tau j}-J_{\theta Yj}-J_{\theta j-\Delta Y}+J_{\theta j+\Delta Y}-J^{\alpha}_{\theta j}-J^{\beta}_{\theta j}-J^{\gamma}_{\theta j}=0 \tag{23}$$

(iv) *Mass equation*:

$$\Delta Y\,Sc\,\mathrm{d}C_j/\mathrm{d}\tau-Sc(C_{j+1}-C_{j-1})/2=(C_{j-1}-C_j)/\Delta Y-(C_j-C_{j+1})/\Delta Y \tag{24}$$

Defining the currents,

$$J_{Cj+1}=(C_j-C_{j+1})/\Delta Y \tag{25a}$$

$$J_{Cj-\Delta Y}=(C_{j-1}-C_j)/\Delta Y \tag{25b}$$

$$J_{Cyj}=Sc(C_{j+1}-C_{j-1})/2 \tag{25c}$$

$$J_{C\tau j}=\Delta Y\,Sc\,\mathrm{d}C_j/\mathrm{d}\tau \tag{25d}$$

DOI: 10.1002/fld

Equation (24) can be expressed in the form of Kirchhoff's law:

$$J_{C\tau j} - J_{CYj} - J_{Cj-1} + J_{Cj+1} = 0 \tag{26}$$

$J_{\Phi\tau j}$ is the transitory term, implemented by means of a capacitor $C_{\Phi j}$ connected to the centre of each cell. $J_{\Phi Yj}$ is the current due the inertia term of V, implemented by means of voltage control current generators $G_{\Phi Yj}$. $J_{\Phi j+1}$ and $J_{\Phi j-1}$ are the currents that leave and enter the cell for the friction term and they are implemented by means of two resistances $R_{\Phi j+1}$ and $R_{\Phi j-1}$ of value ΔY, respectively. Other voltage control current generators ($G^{\alpha}_{\Phi j}, G^{\beta}_{\Phi j}, G^{\gamma}_{\Phi j}$) are employed to implement the buoyancy effect, the viscous dissipation, the internal generation heat, the magnetic field and the angular rotation. Φ_j, Φ_{j+1} and Φ_{j-1} are the voltages of the nodes 'j' (half of the cell), '$j+1$' and '$j-1$' (extremes of the cell), respectively.

Finally, for the initial condition, the voltages $U = N = \theta = C = 0$ for $\tau \leqslant 0$ are applied to the four capacitors $C_{Uj}, C_{Nj}, C_{\theta j}$ and C_{Cj}. To implement the boundary conditions at $Y = 0$, constant voltage sources are employed for the velocity, temperature and concentration, while for the implementation of $N = -m\partial U/\partial Y$, a current control voltage generator is used. The boundary conditions at $Y \to \infty$ are implemented by means of ground elements. A total of N_{cells} (a mesh system with 150 nodes is proven to suggest mesh-independent results) are connected in series to form the network model complete together with the boundary conditions in the extremes.

RESULTS AND DISCUSSION

The results of the numerical computations are shown in Figures 2–8 for distribution of velocity, angular velocity and temperature. Following the above-cited works, we consider the following physically realistic values of the parameters: constant values, $\lambda = 0.5$, $Gm = 2.0$, $B = 0.1$ and other values (ranges) $Pr = 0.7$–10.0, $Gr^* = 2.0$–5.0, $Sc = 0.01$–0.7, $Ec = 0.01$–0.2, $M = 1.0$–8.0, $\Lambda = 0$–5.0, $A = 0$–0.5, $m = 0, 1.0$. The numerical values employed in each case are included in each figure. Figures 2 and 3 show the distribution of the velocity within the boundary layer. Figure 2 shows the transient ($\tau = 0.5, 1.0, 2.0$ and 3.0) and steady-state (the condenser of the network merely has to be omitted) response for two cases, $Pr = 1.0$, $\Lambda = A = 0$ and $Pr = 5.0$, $\Lambda = 5.0$, $A = 0.5$. We observe from this figure that the velocity increases with time to reach the steady state (maximum values). This figure also shows the results obtained by El-Amin [9] with heat generation ($A = 0$) for comparison. The excellent degree of agreement of the present results with those of this author using the fourth-order Runge–Kutta together with a shooting technique can be appreciated. The effects of the magnetic parameter, heat generation parameter and Joule heating are shown in Figure 3, in which it can be seen that a decrease in the magnetic parameter M or an increase in the heat generation parameter A leads to an increase in the velocity, while the location of the maximum velocity moves farther away from the plate. In this same figure, it can be seen that the Joule heating effect leads to a very gradual increase with velocity field.

Figures 4–6 show the distribution of the angular velocity within the boundary layer. Figure 4 shows the transient ($\tau = 0.5, 1.0, 2.0, 3.0, 4.0$ and 5.0) and steady-state response for $\Lambda = 1.0$ and 5.0. As can be seen from this figure, as Λ increases, the amplitude of the angular velocity increases, that is to say, the absolute values increase, and positive values are reached far from the wall and negative values near the wall. These values increase with time to reach the steady state (maximum and minimum values, respectively). The effects of magnetic parameter, heat generation parameter

DOI: 10.1002/fld

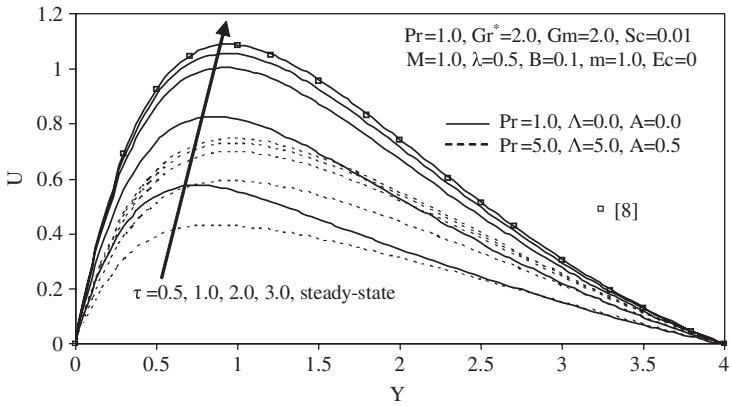

Figure 2. Transient and steady-state dimensionless velocity profiles with $Pr=1.0$, $Gr^*=2.0$, $Gm=2.0$, $Sc=0.01$, $M=1.0$, $\lambda=0.5$, $B=0.1$, $m=1.0$ and $Ec=0$, for $Pr=1.0$ and 5.0, $\Lambda=0.0$ and 5.0, $A=0.0$ and 0.5. Comparison of the results with Reference [8].

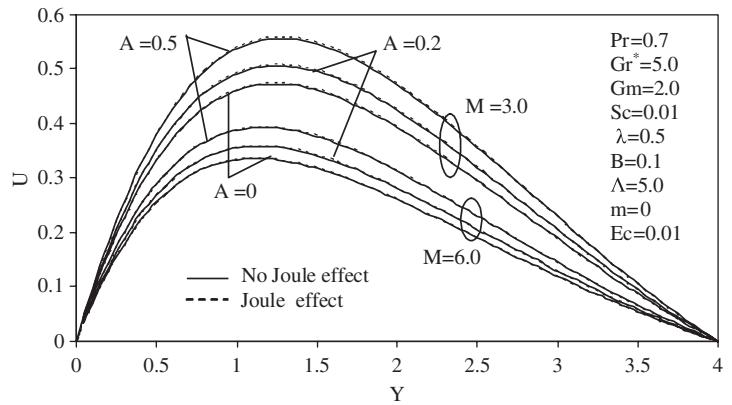

Figure 3. Effects of Joule heating, A and M on the dimensionless velocity profiles with $Pr=0.7$, $Gr^*=5.0$, $Gm=2.0$, $Sc=0.01$, $\lambda=0.5$, $B=0.1$, $\Lambda=5.0$, $m=0$ and $Ec=0.01$.

and Joule heating are shown in Figure 5, in which it can be seen that a decrease in the magnetic parameter M or an increase in the heat generation parameter A leads to an increase in the amplitude of the angular velocity. In the same figure, it can be seen that the Joule heating effect leads to a very gradual increase in the angular velocity field. In Figure 6 the temporal response ($\tau=0.5, 1.0, 2.0$ and steady state) of the angular velocity is plotted. The effects of the Schmidt number and viscous dissipation are analysed. As can be seen, the angular velocity increases as Sc decreases or Ec increases. We observe from this figure that the angular velocity increases with time to reach the steady state.

The transient temperature profiles ($\tau=0.5, 1.0, 2.0$ and steady state) are shown in Figure 7. As Gr^* increases, the temperature profile within the boundary layer tends to increase; in addition, the temperature increases with time to reach the steady state. The stationary response is shown

DOI: 10.1002/fld

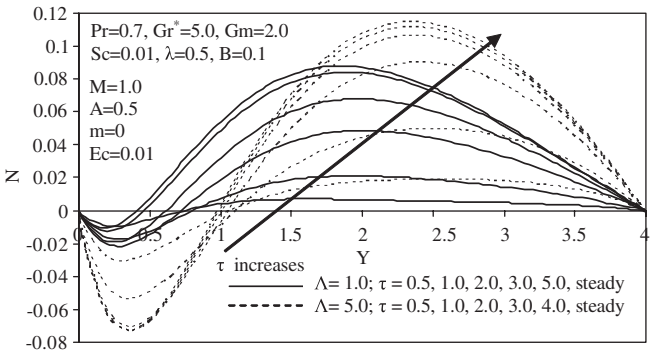

Figure 4. Dimensionless transient and steady-state angular velocity profiles for various values of Λ with $Pr=0.7$, $Gr^*=5.0$, $Gm=2.0$, $Sc=0.01$, $\lambda=0.5$, $B=0.1$, $M=1.0$, $A=0.5$, $m=0$, $Ec=0.01$.

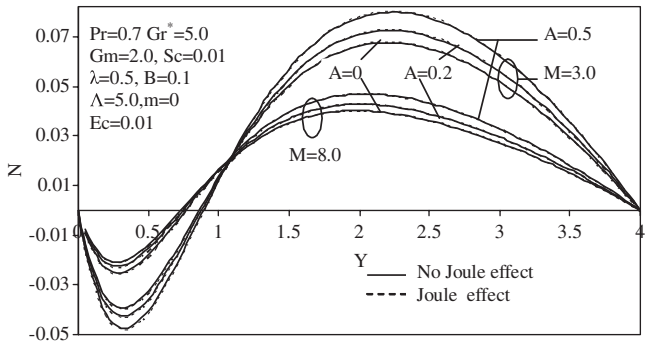

Figure 5. Dimensionless steady-state angular velocity profiles for various values of M and A with $Pr=0.7$, $Gr^*=5.0$, $Gm=2.0$, $Sc=0.01$, $\lambda=0.5$, $B=0.1$, $M=1.0$, $A=0.5$, $m=0$, $Ec=0.01$. Effects of Joule heating.

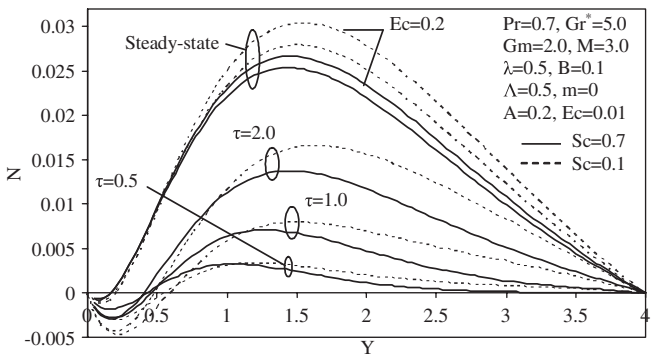

Figure 6. Dimensionless transient and steady-state angular velocity profiles for various values of Sc and Ec with $Pr=0.7$, $Gr^*=5.0$, $Gm=2.0$, $Sc=0.01$, $\lambda=0.5$, $B=0.1$, $M=1.0$, $A=0.5$ and $m=0$.

DOI: 10.1002/fld

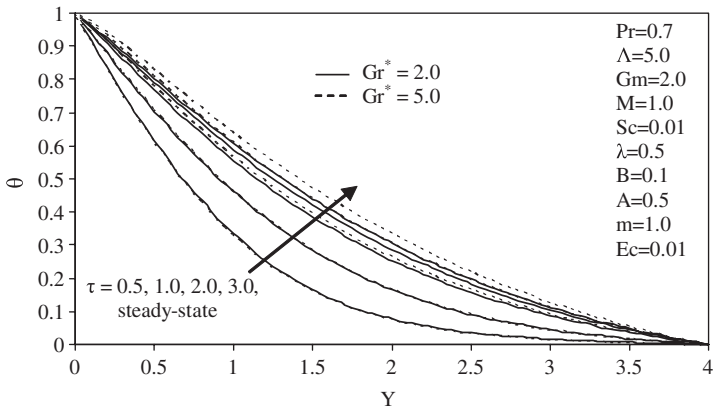

Figure 7. Dimensionless transient and steady-state temperature profiles for various values of Gr^* with $Pr=0.7$, $\Lambda=5.0$, $Gm=2.0$, $M=1.0$, $Sc=0.01$, $\lambda=0.5$, $B=0.1$, $A=0.5$, $m=1.0$ and $Ec=0.01$.

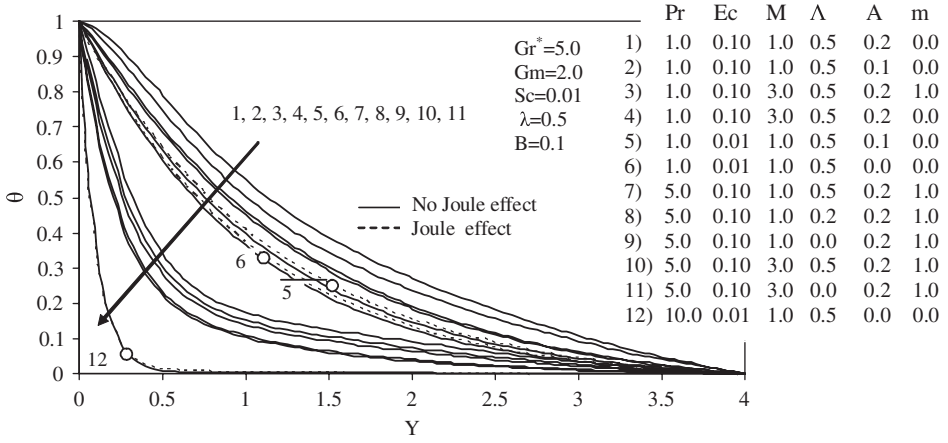

	Pr	Ec	M	Λ	A	m
1)	1.0	0.10	1.0	0.5	0.2	0.0
2)	1.0	0.10	1.0	0.5	0.1	0.0
3)	1.0	0.10	3.0	0.5	0.2	1.0
4)	1.0	0.10	3.0	0.5	0.2	0.0
5)	1.0	0.01	1.0	0.5	0.1	0.0
6)	1.0	0.01	1.0	0.5	0.0	0.0
7)	5.0	0.10	1.0	0.5	0.2	1.0
8)	5.0	0.10	1.0	0.2	0.2	1.0
9)	5.0	0.10	1.0	0.0	0.2	1.0
10)	5.0	0.10	3.0	0.5	0.2	1.0
11)	5.0	0.10	3.0	0.0	0.2	1.0
12)	10.0	0.01	1.0	0.5	0.0	0.0

Figure 8. Dimensionless steady-state temperature profiles for various values of Pr, Λ, M, A, m and Ec with $Gr^*=5.0$, $Gm=2.0$, $Sc=0.01$, $\lambda=0.5$, $B=0.1$.

in Figure 8 as a function of different parameters. It can seen, that as Λ, A, Ec and m increase or as M and Pr decrease, the temperature profile increases. In the same figure, it can be seen that the Joule heating effect leads to an increase in the temperature field; besides, the boundary layer thickness decreases as Pr increases. The concentration distribution, which is affected only by Sc, decreases as this parameter increases (case no plotted).

Tables II–IV show the spatial derivates in the wall ($Y=0$), $U'(0)=\mathrm{d}U/\mathrm{d}Y|_{Y=0}$, $N'(0)=\mathrm{d}N/\mathrm{d}Y|_{Y=0}$, $\theta'(0)=\mathrm{d}\theta/\mathrm{d}Y|_{Y=0}$ and $C'(0)=\mathrm{d}C/\mathrm{d}Y|_{Y=0}$ necessary to determine the local friction factor, the couple stress at the wall, the Nusselt number and the Sherwood number, respectively. Table II shows the results obtained by El-Amin [9] with heat generation ($A=0$) to confirm the accuracy of the results. The values of $U'(0)$, $N'(0)$ and $\theta'(0)$ are very close for high values of M, while the same values are obtained for $C'(0)$.

DOI: 10.1002/fld

Table II. Values of $U'(0)$, $N'(0)$, $\theta'(0)$ and $C'(0)$ for various values of M, Ec and Sc with $\Lambda=1.5$, $Gr=5$, $Gm=2$, $Pr=0.7$, $\lambda=0.5$, $m=0.5$, $B=0.1$, $A=0$ and no effect Joule considered.

			$U'(0)=\mathrm{d}U/\mathrm{d}Y\|_{Y=0}$		$N'(0)=\mathrm{d}N/\mathrm{d}Y\|_{Y=0}$		$-\theta'(0)=-\mathrm{d}\theta/\mathrm{d}Y\|_{Y=0}$		$-C'(0)=-\mathrm{d}C/\mathrm{d}Y\|_{Y=0}$
M	Ec	Sc	[8]	NSM	[8]	NSM	[8]	NSM	[8] and NSM
1.3	0.0	0.0	3.11498	3.07800	3.35721	3.31740	0.74532	0.74532	0.25000
		0.05	3.08916	3.05270	3.33095	3.29172	0.74532	0.74472	0.27583
	0.01	0.0	3.12611	3.10480	3.36888	3.34540	0.72762	0.70183	0.25000
		0.05	3.10000	3.07890	3.34229	3.31900	0.72800	0.70278	0.27583
2.5	0.0	0.0	2.49175	2.49000	2.70253	2.6997	0.74532	0.74532	0.25000
		0.05	2.47465	2.47290	2.68519	2.68240	0.74532	0.74532	0.27583
	0.01	0.0	2.49590	2.50040	2.70690	2.71070	0.73532	0.72019	0.25000
		0.05	2.47871	2.48310	2.68946	2.69320	0.73550	0.72065	0.27583
3.3	0.0	0.0	2.25822	2.24420	2.45594	2.44030	0.74532	0.74532	0.25000
		0.05	2.24407	2.30020	2.44161	2.42610	0.74532	0.74532	0.27583
	0.01	0.0	2.26090	2.25080	2.45876	2.44720	0.73756	0.72614	0.25000
		0.05	2.24669	2.23670	2.44438	2.43290	0.73769	0.72646	0.27583
4.5	0.0	0.0	1.98164	1.98100	2.16272	2.16120	0.74532	0.74532	0.25000
		0.05	1.97069	1.97000	2.15168	2.15020	0.74532	0.74532	0.27583
	0.01	0.0	1.98313	1.98470	2.16430	2.16520	0.73980	0.73147	0.25000
		0.05	1.97216	1.97370	2.15323	2.15410	0.73988	0.73168	0.27583

Comparison of the results with Reference [8].

Table III. Values of $U'(0)$, $N'(0)$, $\theta'(0)$ and $C'(0)$ for various values of M, Λ and A with $Ec=0.02$, $Sc=0$, $Gr=5$, $Gm=2$, $Pr=0.7$, $\lambda=0.5$, $m=0.5$, $B=0.1$. Effects of Joule heating.

M	Λ	A	Effect Joule	$U'(0)$	$N'(0)$	$-\theta'(0)$	$-C'(0)$
1.3	0.5	0.0	Yes	4.33230	4.49440	0.58539	0.25000
		0.0	No	4.18690	4.34480	0.65953	0.25000
		0.2	Yes	4.54260	4.71120	0.43790	0.25000
		0.2	No	4.37290	4.53650	0.52419	0.25000
	1.5	0.0	Yes	3.21440	3.45970	0.60489	0.25000
		0.0	No	3.13300	3.37490	0.65643	0.25000
		0.2	Yes	3.37260	3.62540	0.46078	0.25000
		0.2	No	3.27800	3.52690	0.52061	0.25000
4.5	0.5	0.0	Yes	2.58340	2.68840	0.67675	0.25000
		0.0	No	2.54480	2.64860	0.72170	0.25000
		0.2	Yes	2.67200	2.77980	0.54315	0.25000
		0.2	No	2.62790	2.73430	0.59433	0.25000
	1.5	0.0	Yes	2.01730	2.19950	0.67989	0.25000
		0.0	No	1.98850	2.16920	0.71750	0.25000
		0.2	Yes	2.09300	2.27930	0.54673	0.25000
		0.2	No	2.06000	2.24470	0.58957	0.25000

DOI: 10.1002/fld

Table IV. Values of $U'(0)$, $N'(0)$, $\theta'(0)$ and $C'(0)$ for various values of M, Pr and Ec with $A=0.2, \Lambda=1.5, Sc=0.01, Gr=5, Gm=2, Pr=0.7, \lambda=0.5, m=0.5, B=0.1$. Effects of Joule heating.

M	Pr	Ec	Effect Joule	$U'(0)$	$N'(0)$	$-\theta'(0)$	$-C'(0)$
1.3	0.7	0.00	Yes	3.25120	3.49880	0.59664	0.25503
		0.00	No	3.21150	3.45740	0.62011	0.25503
		0.01	Yes	3.27480	3.52210	0.54880	0.25503
		0.01	No	3.24070	3.48810	0.57173	0.25503
		0.04	Yes	3.54430	3.80870	0.26780	0.25503
		0.04	No	3.33100	3.58160	0.41663	0.25503
	5.0	0.00	Yes	1.90620	2.06150	3.96940	0.25503
		0.00	No	1.88260	2.06320	4.02300	0.25503
		0.01	Yes	1.92780	2.08460	3.86250	0.25503
		0.01	No	1.90400	2.05890	3.91860	0.25503
		0.04	Yes	2.08540	2.25650	3.25600	0.25503
		0.04	No	1.96430	2.12440	3.57230	0.25503
4.5	0.7	0.01	Yes	1.27950	1.40150	3.94570	0.25503
		0.01	No	1.26830	1.38940	3.99110	0.25503
		0.04	Yes	1.32630	1.45270	3.68070	0.25503
		0.04	No	1.27730	1.39920	3.88640	0.25503
	5.0	0.01	Yes	1.27950	1.40150	3.94570	0.25503
		0.01	No	1.26830	1.38940	3.99110	0.25503
		0.04	Yes	1.32620	1.45270	3.68070	0.25503
		0.04	No	1.27730	1.39920	3.88640	0.25503

An increase in the Eckert number Ec and of the heat generation parameter A leads to an increase in the wall shear stress and the wall couple stress, while an increase in the magnetic parameter, couple parameter Λ, Prandtl number Pr and Schmidt number Sc leads to a decrease in the wall shear stress and the wall couple stress. The effect of increasing the values of Ec leads to a decrease in the local Nusselt number, whereas when the viscous dissipation is neglected ($Ec=0$), the heat transfer rate depends only on the Prandtl number and on whether or not the Joule heating effect is considered. Finally, the concentration gradient at the wall depends only on the Schmidt number Sc and increases when Sc increases.

CONCLUDING REMARKS

This paper has presented an unsteady boundary-layer analysis for the flow of a micropolar fluid over a vertical infinite porous plate with exponentially decaying heat generation. The effects of the Prandtl number, magnetic parameter, buoyancy, micropolar parameter, viscous dissipation and Joule heating are analysed. The governing equations are only spatially discretizated and an electrical network model is developed to obtain a numerical solution by means of the PSPICE program. To verify the numerical solution procedure and the computer program, some of the results are compared with those reported in previous works and other new results are added.

DOI: 10.1002/fld

REFERENCES

1. Gebhart B. Effects of viscous dissipation in natural convection. *Journal of Fluid Mechanics* 1962; **14**:225–232.
2. Eringen AC. Theory of micropolar fluids. *Journal of Mathematics and Mechanics* 1966; **16**:1–18.
3. Eringen AC. Theory of thermomicrofluids. *Journal of Mathematical Analysis and Applications* 1972; **38**:480–496.
4. Ibraim FS, Hassanien IA. Mixed convection boundary layer flow of a micropolar fluid on a horizontal flat plate with power law variation in surface temperature. *International Journal of Thermal Science* 2000; **39**:360–373.
5. El-Hakiem MA. Natural convection in a micropolar fluid with thermal dispersion and internal heat generation. *International Communications in Heat and Mass Transfer* 2004; **31**(8):1177–1186.
6. Chang C-L. Numerical simulation of the natural convection plume about line heat source in micropolar fluid. *International Journal of Heat and Mass Transfer* 2006; **49**:3595–3600.
7. Gorla RSR, Takhar HS, Slaout A. Magnetohydrodynamic free convection boundary layer flow of a thermomicropolar fluid over a vertical plate. *International Journal of Engineering Science* 1998; **36**:315–327.
8. Abd El-Hakiem M, Mohammadein AA, El-Kabeir SMM, RSR Gorla. Joule heating effects on magnetohydrodynamic free convection flow of a micropolar fluid. *International Communications in Heat and Mass Transfer* 1999; **26**:219–227.
9. El-Amin MF. Magnetohydrodynamic free convection and mass transfer flow in micropolar fluid with constant suction. *Journal of Magnetism and Magnetic Materials* 2001; **234**:567–574.
10. El-Amin MF. Combined effect of internal heat generation and magnetic field on free convection and mass transfer flow in a micropolar fluid with constant suction. *Journal of Magnetism and Magnetic Materials* 2004; **270**:130–135.
11. Ibrahim FS, Hassanien IA, Bakr AA. Unsteady magnetohydrodynamic micropolar fluid flow and heat transfer over a vertical porous plate through a porous medium in the presence of thermal and mass diffusion with a constant heat source. *Canadian Journal of Physics/Revue Canadienne de Physique* 2004; **82**(10):775–790.
12. Mansour MA, El-Hakiem MA, El Kabeir SM. Heat and mass transfer in magnetohydrodynamic flow of micropolar fluid on a circular cylinder with uniform heat and mass flux. *Journal of Magnetism and Magnetic Materials* 2000; **220**:259–270.
13. Eldabe NT, Ouaf MEM. Chebyshev finite difference method for heat and mass transfer in a hydromagnetic flow of a micropolar fluid past a stretching surface with Ohmic heating and viscous dissipation. *Applied Mathematics and Computation* 2006; **177**:561–571.
14. Abo-Eldahad EM, El Aziz MA. Viscous dissipation and Joule heating effects on MHD-free convection from a vertical plate with power-law variation in surface temperature in the presence of Hall and ion-slip currents. *Applied Mathematical Modelling* 2005; **29**:579–595.
15. PSPICE 6.0. Microsim Corporation, Irvine, CA, 1994.
16. Liskovets OA. The method of lines (Review). *Differential Equations* 1965; **1**:1308–1323.
17. Schiesser WE. *The Numerical Method of Lines. Integration of Partial Differential Equations*. Academic Press: New York, 1991.
18. Zueco Jordán J. Network model to study the transient heat transfer problem in a vertical channel with viscous dissipation. *International Communications in Heat and Mass Transfer* 2006; **33**:1079–1087.
19. Zueco Jordán J. Numerical study of unsteady free convection magneto-hydrodynamic flow of a dissipative fluid along a vertical plate submitted to a constant heat flux. *International Journal of Engineering Science* 2006; **44**:1380–1393.
20. Zueco J, Campo A. Transient radiative transfer between the thick walls of an enclosure using the network simulation method. *Applied Thermal Engineering* 2006; **26**:673–679.
21. Zueco J, Alhama F. Simultaneous inverse determination of the temperature-dependent thermophysical properties of fluids using the network simulation method. *International Journal of Heat and Mass Transfer* 2007; **50**:3234–3243.
22. Nagel LW. SPICE, a computer program to simulate semiconductor circuits. *Memo UCB/ERL M520*, University of California, Berkeley, 1975.

DOI: 10.1002/fld